



Models for skin and brain penetration of major components from essential oils used in aromatherapy for dementia patients

Snezana Agatonovic-Kustrin, Chloe Ke Yi Chan, Vladimir Gegechkori & David W. Morton

To cite this article: Snezana Agatonovic-Kustrin, Chloe Ke Yi Chan, Vladimir Gegechkori & David W. Morton (2019): Models for skin and brain penetration of major components from essential oils used in aromatherapy for dementia patients, Journal of Biomolecular Structure and Dynamics, DOI: [10.1080/07391102.2019.1633408](https://doi.org/10.1080/07391102.2019.1633408)

To link to this article: <https://doi.org/10.1080/07391102.2019.1633408>



Accepted author version posted online: 17 Jun 2019.
Published online: 23 Jun 2019.



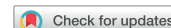
Submit your article to this journal [↗](#)



Article views: 32



View Crossmark data [↗](#)



Models for skin and brain penetration of major components from essential oils used in aromatherapy for dementia patients

Snezana Agatonovic-Kustrin^{a,b} , Chloe Ke Yi Chan^c , Vladimir Gegechkori^b and David W. Morton^{a,b}

^aDepartment of Pharmaceutical and Toxicological Chemistry named after Arzamastsev of the Institute of Pharmacy, I.M. Sechenov First Moscow State Medical University (Sechenov University), Moscow, Trubetskaya, Russia; ^bDepartment of Pharmacy and Biomedical Sciences, La Trobe Institute for Molecular Sciences, La Trobe University, Bendigo, Australia; ^cSchool of Pharmacy, University of Nottingham Malaysia, Semenyih Selangor Darul Ehsan, Malaysia

Communicated by Ramaswamy H. Sarma

ABSTRACT

Aromatherapy with essential oils (EOs) has been linked to improvement of cognitive function in patients with dementia. In order to act systemically, active EO components must be absorbed through the skin, enter the systemic circulation, and cross the blood brain barrier (BBB). Thus, the aim of this work was to develop quantitative structure activity relationships (QSARs), to predict skin and blood barrier penetrative abilities of 119 terpenoids from EOs used in aromatherapy. The first model was based on experimentally measured skin permeability for 162 molecules, and the second model on BBB permeability for 138 molecules. Each molecule was encoded with 63 calculated molecular descriptors and an artificial neural network was used to correlate molecular descriptors to permeabilities. Developed QSAR models confirm that EOs components penetrate through the skin and across the BBB. Some well-known descriptors, such as log P (lipophilicity), molecular size and shape, dominated the QSAR model for BBB permeability. Compounds with the highest predicted BBB penetration were hydrocarbon terpenes with the smallest molecular size and highest lipophilicity. Thus, molecular size is a limiting factor for penetration. Compounds with the highest skin permeability have slightly higher molecular size, high lipophilicity and low polarity. Our work shows that a major disadvantage of novel multitarget compounds developed for the treatment of Alzheimer's disease is the size of molecules, which cause problems in their delivery to the brain. Therefore, there is a need for smaller compounds, which possess more desirable physicochemical properties and pharmacokinetics, in addition to targeted biological effects.

ARTICLE HISTORY

Received 6 April 2019
Accepted 12 June 2019

KEYWORDS

Alzheimer's disease; blood brain barrier; skin penetration; terpenes; QSAR

1. Introduction

Alzheimer's disease (AD), the most common form of dementia, is an age-related progressive neurodegenerative disorder of the central nervous system. As the disease progresses, the brain goes through a progressive shrinking of certain brain areas as the nerve cells die, brain inflammation and cognitive impairment. Microscopic examinations of affected brain tissue show two characteristic pathological hallmarks, extracellular amyloid-beta plaques and intracellular tangles. The formation of the plaques and tangles is associated with the increased activity of enzyme acetylcholinesterase (AChE) leading to reduced levels of neurotransmitter acetylcholine and synaptic alterations. Thus, the main strategy for increasing the cholinergic function in the brain is to inhibit AChE activity. Three out of five medications that are approved by the U.S. FDA, donepezil, galanthamine and rivastigmine, are AChE inhibitors. The fourth drug, memantine is a N-methyl-D-aspartate (NMDA) receptor antagonist. The fifth medication is a combination of one of the cholinesterase inhibitors (donepezil) with memantine. However, the presence of the blood-brain barrier (BBB) limits delivery of these drugs to

the brain. The brain uptake for donepezil (Kim et al., 2010) and rivastigmine (Lee & Kang, 2010) is decreased as the carrier-mediated transport involved in the penetration of these two drugs across the BBB is saturable. Galanthamine being less lipophilic exhibits a very low brain-to-blood concentration ratio (Maelicke, 2018).

Essential oils (EOs) have been used for centuries to ease the symptoms of AD and other dementias. They are well known to possess antioxidant properties and some EOs have been reported to have AChE inhibitory activity (Öztürk, 2012; Wojtunik, Ciesla, & Waksmundzka-Hajnos, 2014). Oxidative stress caused by reactive oxygen species is associated with neurodegenerative conditions, including AD. Therefore, the use of natural compounds with high levels of antioxidants combined with inhibitory activity towards AChE could be an effective therapeutic approach in the treatment of AD. It is established that aromatherapy with EOs of chamomile, lavender, and rosemary can reduce agitated behavior in AD patients. The major constituents of EOs are terpenes and their oxygenated derivatives, the terpenoids. Selected monoterpenoids from thyme, Spanish sage and lavender EOs, are

Table 1. Correlation coefficients, and coefficients of determination (R^2) for the models.

	R_{training}	R_{testing}	RSS	TSS	R^2
Skin model MLP 15(60)-30-1	0.965	0.755	6.32	40	0.842
BBB model MLP 15(56)-4-1	0.845	0.806	32.6	107	0.702

RSS = Residual sum of squares.

TSS = Total sum of squares.

reported to inhibit AChE *in vitro* and some *in vivo* (Houghton, Ren, & Howes, 2006; Mukherjee, Kumar, Mal, & Houghton, 2007; Williams, Sorribas, & Howes, 2011). Many studies, including clinical trials with AD demented patients, have reported beneficial effects from the therapeutic use of EOs (Jimbo, Kimura, Taniguchi, Inoue, & Urakami, 2009; Yoshiyama, Arita, & Suzuki, 2015).

Registration, Evaluation, Authorisation and Restriction of Chemicals (REACH), the European Community Regulation on chemicals and their safe use, recommends the use of *in silico* quantitative structure–activity relationships (QSARs) for preliminary assessment of substances lacking in experimental data (Benfenati et al., 2011). Therefore, the aim of this study was to develop two *in silico* ANN-QSAR models to predict dermal bioavailability and blood brain penetration for major EO components. Due to the vast structural diversity of compounds that are required in order to establish a predictive QSAR model and multiple mechanisms that are involved in skin penetration and blood brain penetration, a non-linear modelling artificial neural network (ANN) approach was used. The ability of ANNs to simultaneously model both linear and non-linear relationships directly from the data makes ANN more successful in finding patterns and complex nonlinear relationships from data sets (Agatonovic-Kustrin, Morton, & Celebic, 2013). QSAR relationships are usually complex, which makes the ANN approach an ideal candidate for QSAR development. In the past, the comparative molecular field analysis (CoMFA) was widely applied, but the nonlinear pattern recognition ability of ANNs was recognized to be better suited in developing QSARs (Kövesdi et al., 1999). ANN QSPR models were also found to be the most statistically relevant when compared to PLS and MLR (Vucicevic, Nikolic, Dobričić, & Agbaba, 2015).

An ANN is a mathematical computational model inspired by the network of biological neurons in the human brain. It learns from examples and errors in a non-linear parallel processing manner. It is composed of a highly connected processing units or artificial neurons that form a network. Artificial neurones are arranged into an input layer (molecular descriptors), an output layer (physical property, in this case Kp or log P) and one or two hidden layers. Artificial neuron is the basic calculating unit that combines weighted sum of the inputs and transforms them into an output using a mathematical function. The standard supervised network architectures (multilayer perceptrons and radial basis functions) are models in which connection weights and number of hidden neurons are adjustable parameters. ANN learns by adjusting interneuron connection weights and by optimizing the number of hidden neurons and hidden layers during the learning phase. This is performed using the training and validation sets of compounds. Training is performed iteratively

such that the ANN will generate a more accurate output and establish a relationship between inputs and output. Following this, true predictive ability of the model can be evaluated on an independent set of compounds.

2. Materials and methods

2.1. Data set and QSAR model building

The skin permeability coefficients, Kp (cm h^{-1}) for 162 out of 171 structurally diverse molecules were taken from Bunge and Vecchia (Bunge & Vecchia, 2002) (Table 1) while the permeability surface area product (PS) data, used as a measure of BBB permeability for 138 out of 153 molecules, were obtained from Suenderhauf, Hammann, and Huwyler (2012) (Table 2). Data for the 119 EO compounds used in this study were collected from several literature sources that describe the chemical compositions of EOs effective in dementia treatment (Nabiha, Abdelfatteh, Faten, Hervé, & Moncef, 2010; Patora, Majda, Gora, & Klimek, 2003; Salido, Altarejos, Nogueras, Saánchez, & Luque, 2003; Shellie, Mondello, Marriott, & Dugo, 2002). 3D molecular structures of both data sets comprising of 163 and 138 molecules respectively, along with 120 EO compounds were downloaded from ChemSpider (www.chemspider.com). The structures of each molecule were then modelled and optimized to minimum energy conformation using the standard geometry minimization procedure MM2 (full molecular mechanics) in Molecular Modelling Pro 6.1. (ChemSW, Fairfield, CA, USA). Each molecule was encoded with 91 calculated descriptors that described 2D and 3D structural information as well as molecular physicochemical properties. These included molecular size and shape parameters (molecular weight, surface area, volume, kappa shape and connectivity indices), electrostatic parameters (dipole moment), valence indices 0–3, lipophilicity parameters (water solubility, polarity, percent hydrophilic surface and hydrophilic–lipophilic balance), hydrogen bonding potential, cyclic components, and specific substitution. Statistica® Neural Networks version 7 (StatSoft Inc., Tulsa) was then used to develop two predictive QSAR models. Calculated molecular descriptors were used as inputs, and skin penetration permeability coefficient (Kp) as output for the first hybrid neural network model, and logPS as output for the second hybrid neural network model. Hybrid neural networks allow more flexibility in the predictions when inputs are a combination of categorical (e.g. functional group count) and quantitative or continuous descriptors (e.g. log P) (Agatonovic-Kustrin et al., 2013).

Data sets were randomly divided into training (80%) and testing (20%) to develop predictive models. The Intelligent Problem Solver (IPS) in Statistica® Neural Networks was used to select the network topology and training algorithms. The IPS follows search algorithms to determine the selection of inputs, the number of hidden units, and other key factors in the network design. These search algorithms are used so that the IPS searches for optimal networks of different types that will have minimal error in prediction. Therefore, 250 runs with different network topologies (Multilayer Perceptron, Radial Basis Function and Generalized Regression

Table 2. Selected molecular descriptors selected by the QSAR models and their sensitivity rankings.

Rank	Skin MLP: 15(60)-30-1	BBB MLP: 15(56)-4-1
1	R=C (number of double bonds)	N in non-aromatic ring
2	Ester	Quaternary carbon (CRRRR)
3	R=N=R (number of nitrogen with two double bonds, including nitro)	O in non-aromatic ring
4	Surface area	Veber oral availability
5	N-non aromatic in ring (the number of nitrogens in non-aromatic rings)	O on aromatic ring (number of phenolic group)
6	Connectivity index of the 3rd order	Carbamide
7	Total energy	Secondary carbon (CHHRR)
8	Valence 0	O next to N
9	Hydrogen bond acceptor	SRR (thioether or dialkyl sulphide)
10	Percentage hydrophilic surface	C aromatic 5 (number of carbons in five membered aromatic rings)
11	LogP	Hansen polarity
12	O on aromatic ring (number of phenolic groups)	Tertiary carbon (CHRRR)
13	Hansen polarity	LogP
14	Hydrogen bond donors	Hydrophilic lipophilic balance (HLB)
15	Hydrophilic surface area	Percent hydrophilic surface

The predicted Kp and logPS values for the EO components are given in Table 3.

Neural Network) with different training algorithms were conducted, with the Multilayer Perceptron (MLP) selected as having the best network topology.

The initial learning rate was set at 0.01 and momentum was set up at 0.3. A maximum number of epochs for iterative algorithms was set to 250 while early stopping conditions were based on the error and set to stop the training when the error fails to improve over time. It is recommended to monitor the selection error for minimum improvement in order to prevent over-learning. Training was performed repeatedly, to ensure that the ANN establishes a close relationship between input and outputs and improve the accuracy of the predictions (Kalra, Kumar, & Waliya, 2016). The training set was used to learn relationships, while the test set functions to optimize the network structure and avoid overtraining (or overfitting) through limiting the complexity of the model (Karolidis, Agatonovic-Kustrin, & Morton, 2010).

The developed ANN models were then used to predict skin permeability coefficients and BBB permeability for 120 compounds representing major constituents of EOs.

2.2. Input selection

The selection of input descriptors is essential in developing an successful QSAR model, with short computational time for effective modelling, and to provide good model interpretability (Agatonovic-Kustrin et al., 2013). The initial ANN models were trained with 91 calculated molecular descriptors, with sensitivity analysis used to prune the inputs. Sensitivity analysis ranks the input variables according to the deterioration in modelling performance that occurs if a given variable is not included in the model. Inputs with constantly low sensitivity or highly variable sensitivity were regarded as insignificant and were progressively eliminated from the network.

In order to optimize network configuration, back propagation using the conjugate-gradient approach method was used (Hsieh, 2009). The initial learning rate was set at 0.01 and momentum was set up at 0.3. A maximum number of epochs for iterative algorithms was set to 250 while early stopping conditions were based on the error and set to stop the training when the error fails to improve over time. It is recommended to monitor the selection error for minimum

improvement in order to prevent over-learning. This whole process was repeated until the model consisted of the smallest subset of molecular descriptors that kept the model's predictive ability (Agatonovic-Kustrin et al., 2013).

3. Results

3.1. ANN modelling

Two separate ANN models with MLP topologies were selected to develop and validate the QSARs. The first QSAR model was developed for the prediction of dermal penetration, whereas the second model was used to predict BBB permeability. For percutaneous absorption or penetration through the skin, the potency of penetration of chemical substances was described by the permeability coefficient Kp, while permeability PS, expressed as logPS, was used for BBB permeability modelling.

BBB is formed by specialized tight junctions between endothelial cells that line brain capillaries to create a highly selective barrier between the brain and the rest of the body. A major problem in drug design is to develop a compound that will cross the BBB. Neuroactive drugs are required to cross the BBB to function. Conversely, drugs that target other parts of the body ideally should not cross the BBB to avoid possible psychotropic side effects. Two gold-standard experimental measures of BBB permeability are logBB (the concentration of drug in the brain divided by concentration in the blood) and logPS. LogPS, is considered as a better measure of BBB permeability as it reflects steady-state, as compounds are directly injected into the internal carotid artery (Suenderhauf et al., 2012).

Both models were validated using an external dataset containing only EO components. With the purpose of ensuring that only meaningful inputs are retained in the final models, descriptors with low sensitivities, were pruned after each training epoch. This process was repeated until the models were developed with the smallest subset of molecular descriptors while retaining adequate predictive accuracy of the network. Good correlation coefficients (*R*) and coefficients of determinations or R-squared (*R*²) were used as a measure of predictive accuracy. Coefficient of determination is a measure of how well the variation in the dependent

Table 3. Predicted permeability constant (Kp) and logPS values of the EO components.

Name	Kp (Model) cm/h	LogPS (Model)	Name	Kp (Model) cm/h	LogPS (Model)
(-)-cis-Sabinol	0.019	-1.63	D-Verbenone	0.0141	-1.79
(+)-Dihydrocarveol	0.0212	-1.58	endo-Fenchol	0.0301	-1.56
(E)-beta-Farnesene	0.112	-1.57	Epicubenol	0.023	-1.68
(E)-beta-Ocimene	0.14	-1.44	Estragole	0.0388	-2.17
(E)-Caryophyllene	0.124	-1.24	Eugenol	0.0131	-2.47
(Z)-beta-Farnesene	0.112	-1.57	Geranyl acetate	0.124	-2.44
(Z)-beta-Ocimene	0.14	-1.44	Globulol	0.0321	-2.38
1,4-Cineole	0.029	-1.89	Heptanoic acid	0.0174	-1.91
1,8-Cineole	0.0389	-1.49	Hexyl 2-methylbutyrate	0.031	-2.37
1-Octen-3-ol	0.0215	-1.7	Hexyl butyrate	0.0288	-2.32
2-Carene	0.136	-0.92	Hexyl isobutyrate	0.0281	-1.68
3-Octanol	0.0314	-1.67	Hexyl tiglate	0.0876	-2.38
3-Octanone	0.0124	-1.64	Isoborneol	0.0311	-2.49
3-Thujanol	0.0326	-1.56	Isobornyl formate	0.0191	-2.21
Alloaromadendrene	0.121	-2.09	Isocaryophyllene	0.126	-1.24
alpha-Bergamotene	0.128	-1.24	iso-Menthone	0.031	-1.53
alpha-Bisabolol	0.0233	-1.31	iso-Menthone	0.0118	-1.51
alpha-Bulnesene	0.127	-1.82	Isopulegol acetate	0.1	-2.57
alpha-Cadinol	0.0227	-1.69	Isopulegone	0.0153	-1.54
alpha-Campholenal	0.0132	-1.86	Isoterpinolene	0.151	-1.66
alpha-Cedrene	0.122	-1.6	Lavandulol	0.0193	-2.02
alpha-Copaene	0.115	-2.1	Lavandulyl acetate	0.0788	-1.58
alpha-Humulene	0.124	-1.53	Lavandulyl isobutyrate	0.152	-2.49
alpha-Murolol	0.0231	-1.69	Lavandulyl isovalerate	0.17	-2.01
alpha-Phellandrene	0.15	-1.66	Limonene	0.148	-1.67
alpha-Pinene	0.137	-0.92	Linalool	0.0232	-1.25
alpha-Pinocarvone	0.0137	-1.82	Linalyl acetate	0.175	-1.69
alpha-Terpinene	0.152	-1.68	m-Cymen-8-ol	0.022	-2.23
alpha-Terpineol	0.0234	-2.24	Menthol	0.0307	-1.54
alpha-Thujene	0.137	-0.92	Menthyl acetate	0.0346	-2.52
Aromadendrene	0.121	-2.09	Myrcene	0.137	-1.44
beta-Bourbonene	0.121	-2.1	Myrtenol	0.0188	-2.38
beta-Caryophyllene	0.127	-1.24	Neoisomenthol	0.031	-1.53
beta-Cubebene	0.121	-2.1	Neo-isopulegol	0.0215	-1.99
beta-Elementene	0.119	-1.16	Neryl acetate	0.123	-2.44
beta-Myrcene	0.137	-1.44	Norbornyl acetate	0.0226	-2.34
beta-Phellandrene	0.148	-1.65	Octen-3-ol	0.0215	-1.7
beta-Pinene	0.136	-0.92	Octyl acetate	0.0289	-2.35
beta-Thujone	0.0115	-1.74	o-Cymene	0.143	-1.63
beta-trans-Ocimene	0.14	-1.44	p-Cymen-8-ol	0.022	-1.79
Bicyclogermacrene	0.124	-1.24	p-Cymene	0.142	-1.63
Bisabolol oxide B	0.0126	-0.96	Perillene	0.093	-2.19
Borneol	0.0301	-1.58	Piperitone	0.0157	-1.53
Bornyl acetate	0.0271	-2.39	p-Menthone	0.0118	-1.52
Calamenene	0.127	-1.79	Pulegone	0.0156	-1.54
Camphene	0.146	-0.92	Sabina ketone	0.0115	-1.3
Camphor	0.0116	-1.5	Sabinene	0.137	-0.92
Carvacrol	0.0328	-1.3	Spathulenol	0.0209	-2.45
Carvone	0.0275	-1.57	Terpinen-4-ol	0.0233	-1.8
Caryophyllene oxide	0.0262	-1.47	Terpinolene	0.151	-1.67
Chrysanthenone	0.011	-2.77	Thuja-2,4 (10)-diene	0.15	-0.93
cis-Carveol	0.0206	-1.61	Thymol acetate	0.0709	-2.34
cis-Chrysanthenol	0.0194	-1.9	Thymol methyl ether	0.0421	-1.12
cis-Linalool oxide	0.0109	-5.76	trans-Carveol	0.0206	-1.61
cis-p-Menth-2-en-1-ol	0.0231	-1.79	trans-Dihydrocarvone	0.0154	-1.54
cis-Sabinene hydrate	0.0329	-1.6	trans-Linalool oxide	0.0109	-5.76
Cumin aldehyde	0.0268	-2.43	trans-Pinocarveol	0.0212	-1.87
D Germacrene	0.122	-1.6	trans-Sabinene hydrate	0.033	-1.6
Daucene	0.128	-1.25	Tricyclene	0.17	-1.68
Dihydrolinalool acetate	0.139	-1.64			

variable can be explained by the independent variable. However, there are no standard guidelines on an acceptable level of predictive accuracy. Henseler has proposed R^2 values of 0.75, 0.50 and 0.25 as substantial, moderate and weak predictive accuracy respectively (Karolidis et al., 2010). Hence, as a rule of thumb for interpreting the strength of relationship, correlation coefficients greater than 0.7 along with an R^2 value greater than 0.5, give good model validity (Roy, Paul, Mitra, & Roy, 2009). The R^2 value for each model was calculated based on the formula:

$$R^2 = 1 - \frac{RSS}{TSS} \quad (1)$$

where RSS is the residual sum of squares and TSS the total sum of squares (Consonni, Ballabio, & Todeschini, 2009) obtained from the analysis of variance (ANOVA) (Table 1).

MLP Neural Networks with an architecture of 15(60)-30-1 and 15(56)-4-1 were selected for dermal and BBB permeability due to their high overall coefficient of correlations (R_{mean}) of 0.862 and 0.826 respectively. The overall correlation of

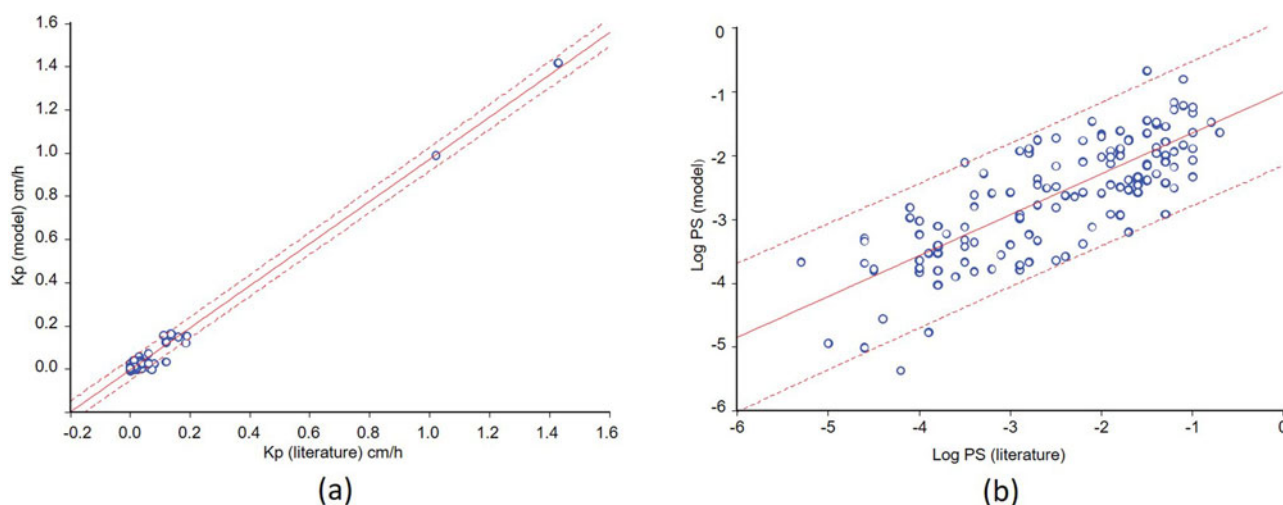


Figure 1. Scatter-plot for (a) Dermal and (b) BBB penetration with 95% prediction interval indicated by the dotted lines.

Table 4. Summary of stepwise regression for the skin permeability model.

Molecular descriptor	Step + in/–out	Multiple R	Multiple R-square	F - to entr/rem	p-level	Equation coefficients
C aromatic 6	1.00	0.23	0.05	9.19	0.00	0.732
O on aromatic	2.00	0.33	0.11	9.02	0.00	–0.414
any N	3.00	0.38	0.14	7.02	0.01	–0.381
O = on aromatic	4.00	0.41	0.17	4.36	0.04	0.115
Urea	5.00	0.42	0.18	2.38	0.12	0.385
N = O	6.00	0.44	0.19	2.68	0.10	0.304
percent hydrophilic surface	7.00	0.46	0.21	3.18	0.08	–5.691
HLB	8.00	0.48	0.23	3.79	0.05	5.358
ester	9.00	0.49	0.24	1.87	0.17	0.195
ORR	10.00	0.51	0.26	3.38	0.07	–0.402
O in nonaromatic ring	11.00	0.51	0.26	1.68	0.20	0.210
N- nonaromatic in ring	12.00	0.52	0.27	1.00	0.32	–0.058
C aromatic 5	13.00	0.53	0.28	1.68	0.20	0.231
OCRO	14.00	0.53	0.29	1.71	0.19	–0.009
molecular width	15.00	0.54	0.30	2.21	0.14	–0.719
ternary carbon atom	16.00	0.58	0.33	7.51	0.01	1.377
C nonaromatic ring	17.00	0.59	0.35	4.40	0.04	–0.778
valence 0	18.00	0.61	0.37	3.65	0.06	1.992
valence 1	19.00	0.62	0.39	4.54	0.03	–1.924
R = N	20.00	0.63	0.40	2.75	0.10	0.250

Table 5. Summary of stepwise regression for the BBB model.

Molecular descriptor	Step + in/–out	Equation coefficients	Multiple R	Multiple R-square	R-square change	F - to entr/rem	p-level
logP	1	0.41	0.59	0.35	0.35	78.96	0.000
hydrophilic surface area	2	–0.44	0.68	0.46	0.11	31.33	0.000
kappa 2	3	–0.54	0.70	0.49	0.03	7.14	0.008
C nonaromatic ring	4	–0.23	0.71	0.51	0.02	4.74	0.031
HOMO	5	1.78	0.74	0.55	0.04	12.32	0.001
LUMO	6	–1.76	0.75	0.56	0.02	6.28	0.013
N = N	7	–0.10	0.76	0.57	0.01	2.42	0.122
N- aromatic single bond	8	0.14	0.76	0.58	0.01	2.95	0.088
total energy	9	0.29	0.77	0.59	0.01	2.52	0.114
any S	10	–0.11	0.77	0.60	0.01	3.87	0.051
valence index 4	11	–0.56	0.78	0.61	0.01	2.52	0.114
valence 1	12	0.73	0.79	0.62	0.01	4.14	0.044
molecular weight	13	–0.85	0.79	0.62	0.00	1.65	0.201
any C	14	–0.13	0.79	0.63	0.00	1.60	0.207
connectivity 1	15	2.26	0.79	0.63	0.00	1.14	0.288
connectivity index 4	16	–1.06	0.80	0.64	0.01	2.96	0.088
H bond acceptor	17	0.31	0.80	0.64	0.00	1.72	0.192
dipole moment	18	–0.25	0.81	0.66	0.02	6.04	0.015

BBB permeability model is however, slightly lower than that of the skin model probably due to the high diversity of the molecular structures that was used to establish the model.

The hybrid ANN models were built from a combination of categorical and continuous descriptors. These descriptors

could be classified in four main groups as solubility/permeability descriptors (e.g. logP, Hansen polarity, hydrogen bond donors), topological descriptors (e.g. double bond (R = C), quaternary carbon (CRRRR), surface area (SA)), functional group counts and quantum-chemical descriptors (e.g. total energy).

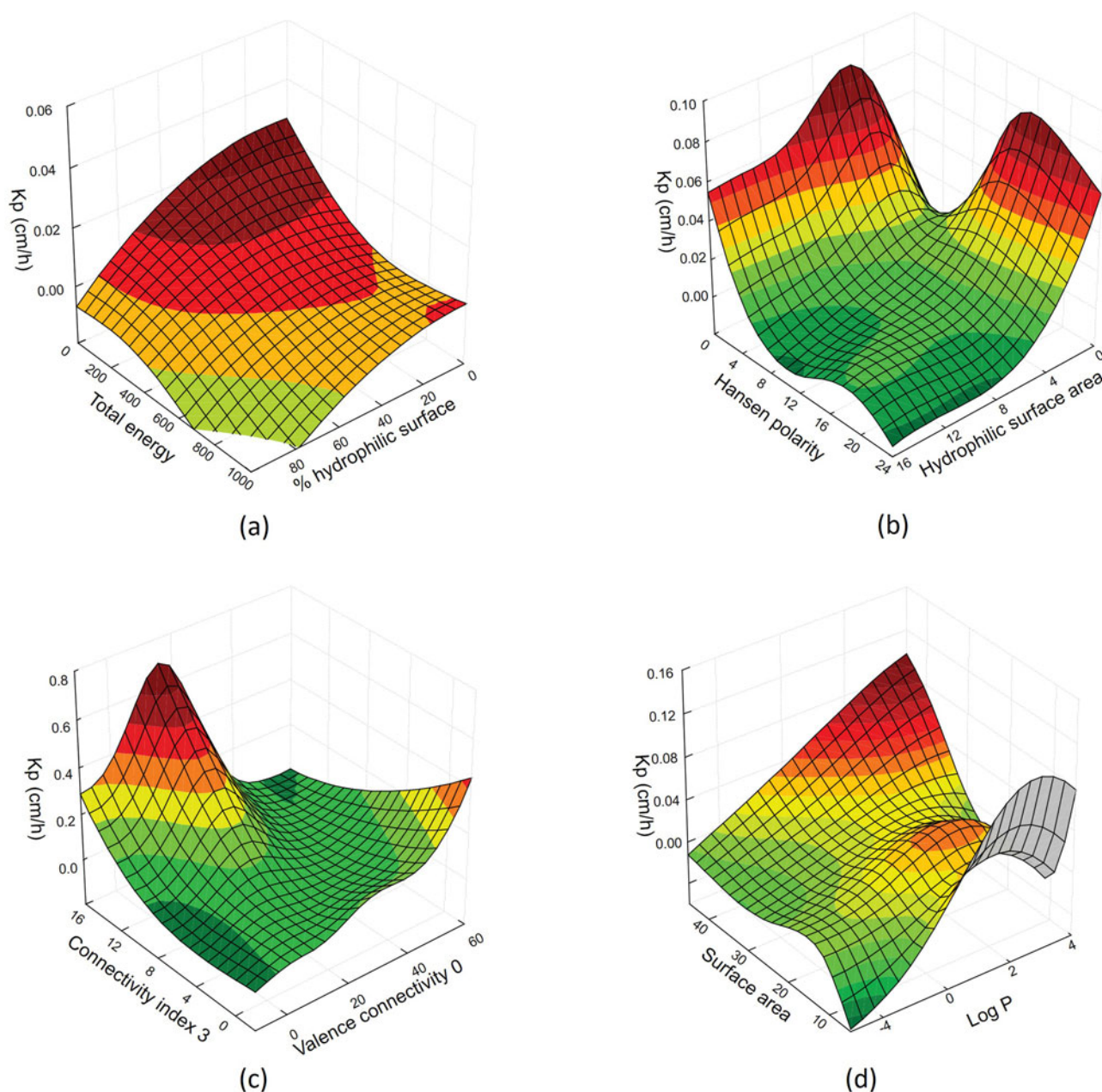


Figure 2. Response graph of Kp (skin penetration constant) versus selected molecular descriptors.

Table 2 displays the selected molecular descriptors of skin and BBB models, and their sensitivity rankings.

Scatter plots of observed against predicted values for compounds used to build models (training and testing data) show that data points for both models are mostly located within the 95% confidence interval (Figure 1).

3.2. Multiple linear regression (MLR) modelling

The predictive ability of the ANN was compared with a MLR model using the same training/testing data sets. Stepwise regression was employed to develop a regression equation that would correlate the permeability constant (Kp) for training and testing sets with molecular descriptors. A multiple forward stepwise regression (SW-MLR) method was used to select input variables (molecular descriptors) that best

describe permeability constant. The initial step was to build a model with a single independent variable and the dependent variable, and then the model was repeatedly altered by adding one independent variable (molecular descriptor) at a time until the relationship was no longer improved. Although we have used stepwise regression to refine the model and to select the most important descriptors, the final equation (Equation 2) is too cumbersome with 20 molecular descriptors required for the skin permeability model (Table 4) and 18 molecular descriptors required for the BBB model (Equation 3 and Table 5). The combination of selected descriptors gave the squared regression coefficients for training/testing sets of 0.77/0.55 and 0.84/0.78 for the skin permeability and BBB models respectively. The results revealed that the developed ANN model produced more accurate predictions of skin permeability constant (Kp) and permeability

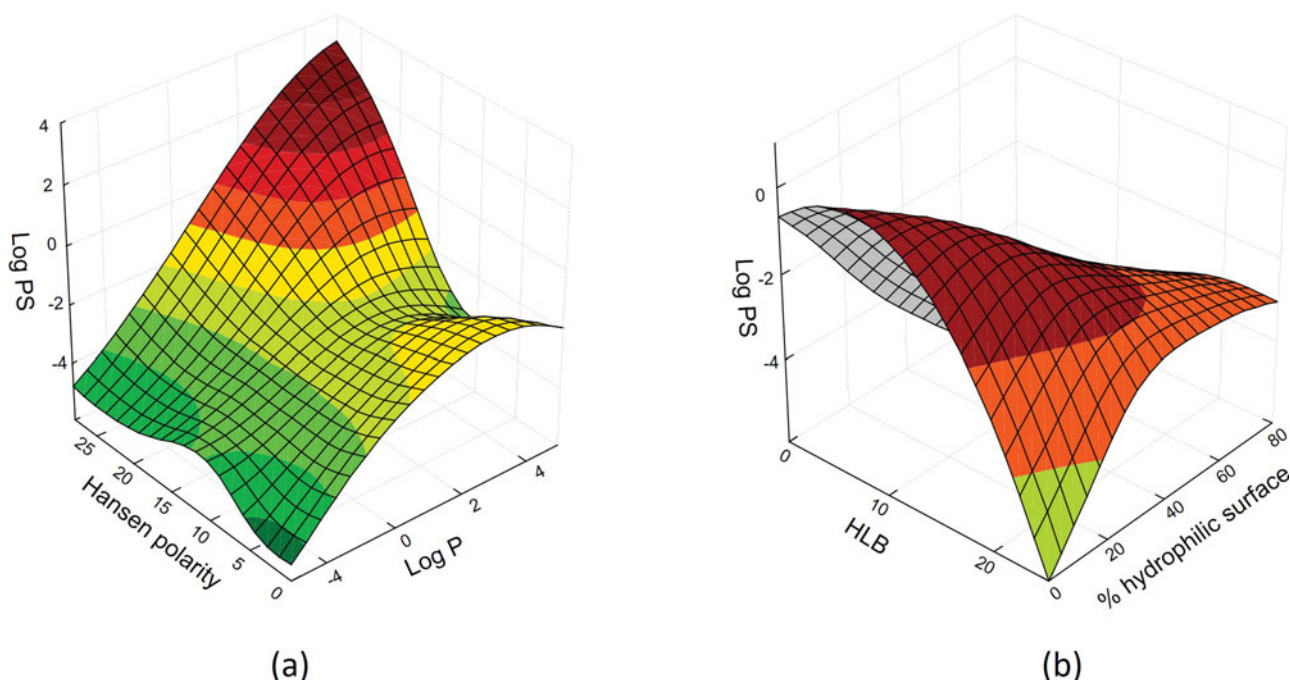


Figure 3. Response surface of LogPS against (a) Hansen polarity and logP; (b) HLB and % hydrophilic surface.

PS expressed as logPS. This confirms previous work that reported that predictive ability of ANNs in modelling blood barrier penetration was superior to linear computational modelling approaches (Garg & Verma, 2006).

R = regression coefficient. F value for a variable indicates its statistical significance. It is a measure of the extent to which a variable makes a unique contribution to the prediction of group membership. p -level represents probability of error involved in accepting hypothesis that the differences between the parameter estimates are equal to zero, and hence, that they are of equal magnitude. Specifically, the coefficients are used to form linear combinations of parameter estimates, and these linear combinations are then tested against zero.

$$K_p = 0.732 \times (\text{\# of aromatic six membered rings}) - 0.41 \times (\text{\# of phenolic-OH groups}) - 0.38 \times (\text{\# of nitrogens}) + 0.115 \times (\text{\# of aromatic ketones}) + 0.385 \times (\text{\# of urea groups}) - 5.7 \times (\text{\% hydrophilic surface}) + 5.36 \times (\text{HLB}) + 0.195 \times (\text{\# of ester groups}) - 0.40 \times (\text{\# of ether groups}) + 0.21 \times (\text{\# of oxygens in nonaromatic rings}) - 0.058 \times (\text{\# of nitrogens in nonaromatic rings}) + 0.231 \times (\text{\# carbons in 5-membered aromatic rings}) - 0.01 \times (\text{\# carbon in between 2 oxygens}) - 0.72 \times (\text{molecular width}) + 1.38 \times (\text{tertiary carbon atom}) - 0.78 \times (\text{\# carbons in nonaromatic rings}) + 1.99 \times (\text{valence index O}) - 1.9 \times (\text{valence index 1}) + 0.25 \times (\text{\# of double bonded nitrogens (including aromatic)}) (2)$$

$$\log PS = 0.41 \times (\log P) - 0.44 \times (\text{hydrophilic surface area}) - 0.54 \times (\text{kappa 2}) - 0.23 \times (\text{\# of C in nonaromatic ring}) + 1.78 \times (\text{HOMO}) - 1.8 \times (\text{LUMO}) - 0.10 \times (\text{\# of diazo groups}) + 0.14 \times (\text{\# of aromatic amino groups}) + 0.29 \times (\text{total energy}) - 0.11 \times (\text{\# of S atoms}) - 0.56 \times (\text{valence index 4}) + 0.73 \times (\text{valence 1}) - 0.85 \times (\text{molecular weight}) - 0.13 \times (\text{\# of C atoms}) + 2.26 \times (\text{connectivity index 1st order}) - 1.1 \times (\text{connectivity index 4th order}) + 0.31 \times (\text{\# of hydrogen bond acceptors}) - 0.25 \times (\text{dipole moment}) (3)$$

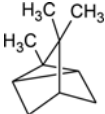
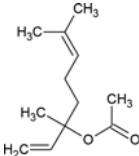
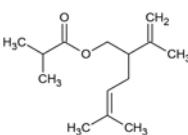
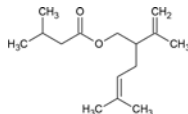
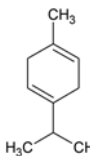
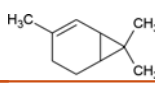
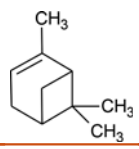
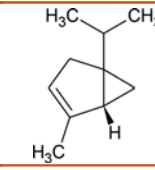
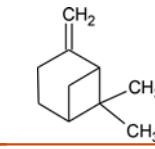
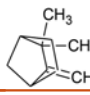
4. Discussion

Although different models may give regressions with similar statistical accuracy, the selection of descriptors should be related to the models and be easily interpretable. It is well established that important factors playing a part in dermal absorption are the physical and chemical properties of a compound, including its molecular weight, solubility, partitioning coefficient, acid dissociation constant (pKa) and the condition of the skin.

The skin is composed of two layers: a nonvascular epidermis and a highly vascularized dermis. The outermost layer of the epidermis, the stratum corneum provides an absorption barrier. For most compounds, the rate of dermal absorption is limited by diffusion through the stratum corneum. Penetration can be increased if compounds can damage or partially dissolve the stratum corneum. Natural terpenes, the main constituents of EOs, have been long used as skin penetration enhancers in transdermal drug delivery systems (Herman & Herman, 2015). Terpenes are small, highly lipophilic molecules, composed of only carbon, hydrogen and oxygen atoms. It has been suggested that terpenes disrupt the structure of the intercellular lipids of the stratum corneum (Godwin & Michniak, 1999). The effect of a specific terpene on skin depends on its chemical structure and physicochemical properties, such as its lipophilicity, size and chirality, degree of unsaturation.

The model suggests the best penetrants are those that are soluble in both lipids and water, whereas compounds that are largely soluble only in either lipids or water, but not both, are poorer penetrants. However, permeability constant (K_p values) tend to increase with increasing lipophilicity of the terpenes in the following order; oxides < ketones < alcohols < esters. The lowest skin penetration was predicted for the stereoisomers of

Table 6. Compounds with the highest predicted dermal and BBB penetration.

	Name	Tricyclene	Linalyl acetate	Lavandulyl isobutyrate	Lavandulyl isovalerate	Terpinene
						
Highest dermal penetration	Structure					
	Molar mass	136.24	196.29	224.34	238.37	136.24
	Molecular volume/ \AA^3	58.21	101.58	113.48	120.87	71.09
	Surface area/ \AA^2	8.94	14.93	16.84	17.79	10.14
	LogP	4.30	3.34	4.35	4.88	4.23
	HLB	0.00	0.92	2.22	1.99	0.00
	Hansen polarity	0.00	2.27	1.98	1.86	0.00
	Percent hydrophilic surface	0.00	10.35	16.01	15.01	0.00
	Connectivity 3	5.24	3.32	4.19	3.96	3.00
	Valence 0	23.15	29.59	35.17	37.88	23.15
	Hydrophilic surface area/ \AA^2	0.00	1.54	2.70	2.67	0.00
	Polar surface area/ \AA^2	0.00	29.46	29.46	29.46	0.00
	Name	2-carene	α -pinene	α -thujene	β -pinene	camphene
						
Highest BBB permeability	Structure					
	Molar volume	136.24	136.24	136.24	136.24	136.24
	Molecular volume/ \AA^3	65.97	64.10	64.01	67.58	70.84
	Surface area/ \AA^2	9.78	9.47	9.48	9.64	9.93
	LogP	4.47	4.56	4.06	4.21	4.34
	HLB	0.00	0.00	0.00	0.00	0.00
	Hansen polarity	0.00	0.00	0.00	0.00	0.00
	Percent hydrophilic surface	0.00	0.00	0.00	0.00	0.00
	Connectivity 3	3.75	4.20	3.88	4.20	4.41
	Valence 0	23.15	23.15	23.15	22.98	22.98
	Hydrophilic surface area/ \AA^2	0.00	0.00	0.00	0.00	0.00
	Polar surface area/ \AA^2	0.00	0.00	0.00	0.00	0.00

linalool oxide and sabina ketone, while the highest skin penetration was predicted for lavandulyl and linalyl esters.

The most important descriptors for skin penetration are molecular shape (connectivity index of the third order), molecular size (surface area), flexibility (presence of double bonds), connectivity index of the third order, and valence connectivity index of the zero order. Molecular unsaturation reflects the flexibility of the molecules (Hückel, 1931) as the sp^2 hybridization state restricts bond rotation and allows a single molecular conformation. Higher molecular connectivity indices include information about the size-dependent degree of carbon branching, while the valence indices add information about heteroatoms (Contrera, MacLaughlin, Hall, & Kier, 2005). Zero order valence index ($^0\chi^v$) despite being a connectivity index, ignores the branching aspect of the molecule and contains information about heteroatoms in the molecule, while higher order valence indices contain the information about molecular volume and molecular surface area. The values of $^0\chi^v$ index increase with the increase in length and branches of hydrocarbon chains, and its values are smaller for the compounds containing in their structure heteroatoms, in comparison with those of their hydrocarbon analogous compounds. Valence index of zero order could also help to differentiate between terpenes (hydrocarbons) and terpenoids (oxygenated derivatives).

Therefore, descriptors such as valence index of zero order, the number of nitrogens in non-aromatic rings, phenolic groups, ester functional groups and hydrogen bond acceptors are important descriptors in the model for dermal permeability.

Total energy is a quantum-chemical descriptor (the sum of kinetic energies and potential energies of a molecule; Pasha, Srivastava, & Singh, 2005), and is related to molecular reactivity. The smaller the total energy, the higher dermal penetration.

The descriptors selected by the BBB model, suggest that carrier mediated transport may be involved in penetration across the BBB. The model indicates the importance of the secondary, tertiary and quaternary carbons (CHRRR, CHRRR, CRRRR) in the molecular structure of EO components due to the specificity in their molecular conformations and chirality. Primary, secondary, tertiary and quaternary carbon atoms make different contributions to the total surface area of the molecule (Cammarata, 1979) and discrimination between carbon atoms should be considered. Veber oral bioavailability descriptors seem also to be very important for molecular penetration of the BBB. According to Veber et al., oral bioavailability is the number of rotatable bonds, and is an indication of molecular flexibility (Veber, Johnson, Cheng, Smith, Ward, & Kopple, 2002).

The number of carbons in five membered aromatic rings indicates the importance of heterocyclic compounds. The

planarity of the aryl ring (C aromatic 5) contributes to the fitting ability of the components to their binding pockets through pi–pi interactions, while heteroatoms can act as bond donors. The presence of heteroatoms, thus may be important in binding to the transport proteins along the BBB. Although the exact transport process of EO components is unclear, carrier mediated transport should be considered for the endothelial cells lining the BBB as they contain a reservoir of transport proteins (Gabathuler, 2010).

It is well established that the main factors affecting membrane permeability of a compound are its lipophilicity and protonation state. Due to the high lipophilicity of the stratum corneum and the BBB, molecules with higher lipophilicity penetrate better through the skin or across the BBB (Figure 3a). However, lipophilicity is not the main determinant for either skin or BBB penetration, suggesting that the process of penetration through both the skin and BBB is much more complex than simple diffusion. The capacity of a substance to penetrate biologic barriers is dependent also on the polarity of a compound and the extent of its non-symmetrical distribution of electron density. Hansen polarity and percent of hydrophilic area are negatively correlated to penetration. The highly nonlinear correlation between descriptors and K_p or $\log PS$ suggest the need for non-linear modelling of dermal penetration (Figure 2).

The model predicted that terpenes (consisting only of carbon and hydrogen), with the smallest molecular size (i.e. lowest molecular weight of 136.24 g/mol , lowest molar volume of $66.32 \pm 2.5 \text{ \AA}^3$, and lowest surface area of $9.66 \pm 0.18 \text{ \AA}^2$) had the highest BBB penetration among investigated EO components (Table 6). These molecules also exhibit the highest lipophilicity ($\log P = 4.33 \pm 0.18$) with $HLB = 0$ and lack of hydrophilic surface area, indicating completely lipophilic molecules that penetrates BBB via passive diffusion. Although it was predicted that terpene tricyclene has high dermal penetration, the BBB model did not predict its high penetration over the brain barrier, although it meets requirements of small size/volume, high lipophilicity and lack of polar surface area. Tricyclene has higher connectivity index of the third order. Since the molecular connectivity indices contain information about the molecular structure, higher value of the third-order connectivity index might indicate unfavorable shape of the molecule for BBB penetration. Compounds with the highest skin permeability have a slightly higher molecular size with a surface area of $13.73 \pm 3.98 \text{ \AA}^2$, a high lipophilicity ($\log P = 4.22 \pm 0.56$), low polarity (polar surface area ~ 0), $HLB \sim 1$, and approximately 8% of hydrophilic surface area. Therefore, a slightly polar molecular surface area is beneficial for dermal penetration.

The terpenoids with the highest dermal penetrative abilities are found to be linalyl acetate, lavandulyl isobutyrate and lavandulyl isovalerate and terpinene. Linalyl acetate is the major constituent of the lavender oil (51%) (Godwin & Michniak, 1999). Components from lavender oils are known to affect cholinergic, dopaminergic, glutamate, opioidergic, and γ -aminobutyric acid (GABA) neurotransmission. These effects are observed shortly after topical application or inhalation of lavender oil (Hückel, 1931). However, there is limited

information on the rate of absorption of lavender oil following aromatherapy treatment.

Electrophysiological studies show that certain EO aromas affect spontaneous brain activities and cognitive functions. Altered electrical activity of the brain after exposure to certain EOs help to explain the psychophysiological activities of EO aroma (Pasha et al., 2005). Altered brain waves activities are responsible for various states of the brain (Cammarata, 1979). This provides further confirmation on how EOs from sage, lavender, bergamot, rosemary and melissa exhibit effective in vivo treatment of dementia symptoms.

5. Conclusions

There is no doubt that components from EOs can be absorbed through the skin, enter into the systemic circulation and then cross the BBB. Therefore, topical application or inhalation of EOs may produce an effect on the nervous system that is not purely psychological. Developed QSAR models confirm that components from EOs penetrate through the skin and across the BBB. Some well-known descriptors, such as $\log P$ (lipophilicity), molecular size and shape were found to dominate the QSAR model for the BBB. The major disadvantage of the novel multi-target-directed ligands for the treatment of Alzheimer disease is the size of molecules, which cause problems in their delivery to the brain (Agatonovic-Kustrin, Kettle, & Morton, 2018). Thus, there is a need for compounds, which possess more desirable physico-chemical properties and suitable pharmacokinetics, in addition to targeted biological effects.

Disclosure statement

No potential conflict of interest was reported by the authors.

Funding

This work did not receive any external funding.

ORCID

Snezana Agatonovic-Kustrin  <http://orcid.org/0000-0002-7714-5510>

Chloe Ke Yi Chan  <http://orcid.org/0000-0002-6273-5825>

References

- Agatonovic-Kustrin, S., Kettle, C., & Morton, D. W. (2018). A molecular approach in drug development for Alzheimer's disease. *Biomedicine & Pharmacotherapy*, 106, 553–565. doi:10.1016/j.biopha.2018.06.147
- Agatonovic-Kustrin, S., Morton, D. W., & Celebic, D. (2013). QSAR: An in silico approach for predicting the partitioning of pesticides into breast milk. *Combinatorial Chemistry & High Throughput Screening*, 16(3), 223–232. doi:10.2174/1386207311316030007
- Benfenati, E., Diaza, R. G., Cassano, A., Pardoe, S., Gini, G., Mays, C., ... Benighaus, L. (2011). The acceptance of in silico models for REACH: Requirements, barriers, and perspectives. *Chemistry Central Journal*, 5(1), 58. doi:10.1186/1752-153X-5-58

- Bunge, A., & Vecchia, B. (2002). Skin Absorption Databases and Predictive Equations. In R. H. Guy, & J. Hadgraft (Eds.), *Transdermal drug delivery* (2 ed., pp. 57–141). New York: Marcel Dekker, Inc.
- Cammarata, A. (1979). Molecular topology and aqueous solubility of aliphatic alcohols. *Journal of Pharmaceutical Sciences*, 68(7), 839–842.
- Consonni, V., Ballabio, D., & Todeschini, R. (2009). Comments on the definition of the Q2 parameter for QSAR validation. *Journal of Chemical Information and Modeling*, 49(7), 1669–1678. doi:10.1021/ci900115y
- Contrera, J. F., Maclaughlin, P., Hall, L. H., & Kier, L. B. (2005). QSAR modeling of carcinogenic risk using discriminant analysis and topological molecular descriptors. *Current Drug Discovery Technologies*, 2(2), 55–67. doi:10.2174/1570163054064684
- Gabathuler, R. (2010). Approaches to transport therapeutic drugs across the blood–brain barrier to treat brain diseases. *Neurobiology of Disease*, 37(1), 48–57. doi:10.1016/j.nbd.2009.07.028
- Garg, P., & Verma, J. (2006). In silico prediction of blood brain barrier permeability: An artificial neural network model. *Journal of Chemical Information and Modeling*, 46(1), 289–297. doi:10.1021/ci050303i
- Godwin, D. A., & Michniak, B. B. (1999). Influence of drug lipophilicity on terpenes as transdermal penetration enhancers. *Drug Development and Industrial Pharmacy*, 25(8), 905–915. doi:10.1081/DDC-100102251
- Herman, A., & Herman, A. P. (2015). Essential oils and their constituents as skin penetration enhancer for transdermal drug delivery: A review. *Journal of Pharmacy and Pharmacology*, 67(4), 473–485. doi:10.1111/jphp.12334
- Houghton, P. J., Ren, Y., & Howes, M. J. (2006). Acetylcholinesterase inhibitors from plants and fungi. *Natural Product Reports*, 23(2), 181–199. doi:10.1039/b508966m
- Hsieh, W. W. (2009). *Machine learning methods in the environmental sciences: Neural networks and kernels*. Cambridge: Cambridge University Press.
- Hückel, E. (1931). Quantentheoretische Beiträge zum Benzolproblem. I. Die Elektronenkonfiguration des Benzols und verwandter Verbindungen. *Zeitschrift für Physik*, 70, 204–286.
- Jimbo, D., Kimura, Y., Taniguchi, M., Inoue, M., & Urakami, K. (2009). Effect of aromatherapy on patients with Alzheimer's disease. *Psychogeriatrics*, 9(4), 173–179. doi:10.1111/j.1479-8301.2009.00299.x
- Kalra, A., Kumar, S., & Waliya, S. S. (2016). ANN training: A survey of classical and soft computing approaches. *IJCTA*, 9(34), 715–736.
- Karolidis, D. A., Agatonovic-Kustrin, S., & Morton, D. W. (2010). Artificial neural network (ANN) based modelling for D1 like and D2 like dopamine receptor affinity and selectivity. *Medicinal Chemistry*, 6(5), 259–270. doi:10.2174/157340610793358891
- Kim, M. H., Maeng, H. J., Yu, K. H., Lee, K. R., Tsuruo, T., Kim, D. D., ... Chung, S. J. (2010). Evidence of carrier-mediated transport in the penetration of donepezil into the rat brain. *Journal of Pharmaceutical Sciences*, 99(3), 1548–1566. doi:10.1002/jps.21895
- Kövesdi, I., Domínguez-Rodríguez, M. F., Örfi, L., Náray-Szabó, G., Varró, A., Papp, J. G., & Mátyus, P. (1999). Application of neural networks in structure–activity relationships. *Medicinal Research Reviews*, 19(3), 249–269.
- Lee, N.-Y., & Kang, Y.-S. (2010). The inhibitory effect of rivastigmine and galantamine on choline transport in brain capillary endothelial cells. *Biomolecules & Therapeutics*, 18(1), 65–70. doi:10.4062/biomolther.2010.18.1.065
- Maelicke, A. (2018). Enhanced brain bioavailability of galantamine by selected formulations and transmucosal administration of lipophilic prodrugs. European Union: Neurodyn Life Sciences Inc.
- Mukherjee, P. K., Kumar, V., Mal, M., & Houghton, P. J. (2007). Acetylcholinesterase inhibitors from plants. *Phytomedicine*, 14(4), 289–300. doi:10.1016/j.phymed.2007.02.002
- Nabiha, B., Abdelfatteh, E. O., Faten, K., Hervé, C., & Moncef, C. M. (2010). Chemical composition of bergamot (*Citrus bergamia* Risso) essential oil obtained by hydrodistillation. *Journal of Chemistry and Chemical Engineering*, 4(4), 60–62.
- Öztürk, M. (2012). Anticholinesterase and antioxidant activities of Savoury (*Satureja thymbra* L.) with identified major terpenes of the essential oil. *Food Chemistry*, 134(1), 48–54. doi:10.1016/j.foodchem.2012.02.054
- Pasha, F. A., Srivastava, H. K., & Singh, P. P. (2005). Comparative QSAR study of phenol derivatives with the help of density functional theory. *Bioorganic & Medicinal Chemistry Letters*, 13(24), 6823–6829.
- Patora, J., Majda, T., Gora, J., & Klimek, B. (2003). Variability in the content and composition of essential oil from lemon balm (*Melissa officinalis* L.) cultivated in Poland. *Acta Poloniae Pharmaceutica*, 60(5), 395–400.
- Roy, P. P., Paul, S., Mitra, I., & Roy, K. (2009). On two novel parameters for validation of predictive QSAR models. *Molecules (Basel, Switzerland)*, 14(5), 1660–1701. doi:10.3390/molecules14051660
- Salido, S., Altarejos, J., Nogueras, M., Saánchez, A., & Luque, P. (2003). Chemical composition and seasonal variations of rosemary oil from Southern Spain. *Journal of Essential Oil Research*, 15(1), 10–14. doi:10.1080/10412905.2003.9712248
- Shellie, R., Mondello, L., Marriott, P., & Dugo, G. (2002). Characterisation of lavender essential oils by using gas chromatography–mass spectrometry with correlation of linear retention indices and comparison with comprehensive two-dimensional gas chromatography. *Journal of Chromatography A*, 970(1–2), 225–234. doi:10.1016/S0021-9673(02)00653-2
- Suenderhauf, C., Hammann, F., & Huwyler, J. (2012). Computational prediction of blood–brain barrier permeability using decision tree induction. *Molecules*, 17(9), 10429–10445. doi:10.3390/molecules170910429
- Veber, D. F., Johnson, S. R., Cheng, H.-Y., Smith, B. R., Ward, K. W., & Kopple, K. D. (2002). Molecular properties that influence the oral bioavailability of drug candidates. *Journal of Medicinal Chemistry*, 45(12), 2615–2623. doi:10.1021/jm020017n
- Vucicevic, J., Nikolic, K., Dobričić, V., & Agbaba, D. (2015). Prediction of blood–brain barrier permeation of α -adrenergic and imidazoline receptor ligands using PAMPA technique and quantitative-structure permeability relationship analysis. *European Journal of Pharmaceutical Sciences*, 68, 94–105. doi:10.1016/j.ejps.2014.12.014
- Williams, P., Sorribas, A., & Howes, M. J. (2011). Natural products as a source of Alzheimer's drug leads. *Natural Product Reports*, 28(1), 48–77. doi:10.1039/c0np00027b
- Wojtunik, K. A., Ciesla, L. M., & Waksmundzka-Hajnos, M. (2014). Model studies on the antioxidant activity of common terpenoid constituents of essential oils by means of the 2, 2-diphenyl-1-picrylhydrazyl method. *Journal of Agricultural and Food Chemistry*, 62(37), 9088–9094. doi:10.1021/jf502857s
- Yoshiyama, K., Arita, H., & Suzuki, J. (2015). The effect of aroma hand massage therapy for people with dementia. *Journal of Alternative and Complementary Medicine*, 21(12), 759–765. doi:10.1089/acm.2015.0158